Geoderma 462 (2025) 117504

Contents lists available at ScienceDirect

Geoderma

journal homepage: www.elsevier.com/locate/geoderma

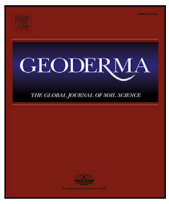

The effect of uncertainty in predictions of nutrient concentrations from soil spectra on variable-rate fertilizer applications

T.S. Breure [a,b,*], R. Webster [a], S.M. Haefele [a], J.A. Hannam [b], R. Corstanje [b], A.E. Milne [a]

[a] Rothamsted Research, Harpenden AL5 2JQ, Great Britain, United Kingdom
[b] Cranfield University, Cranfield, Bedfordshire MK43 0AL, Great Britain, United Kingdom

ARTICLE INFO

Handling Editor: Budiman Minasny

Keywords:
Precision agriculture
Proximal soil-sensing
Soil spectroscopy z
X-ray fluorescence
Geostatistics
Simulation

ABSTRACT

The concentrations of available phosphorus (P) and potassium (K) in soil can be estimated by soil spectroscopy, and with sufficient sampling can be mapped to guide farmers to apply fertilizer at variable rates. Mapping errors arise from both spatial variation and calibration of the spectra against chemically determined concentrations. We aimed to develop a loss-function framework to explore how sizes of sample sets and calibration sets affect the likely profitability of variable-rate applications of P and K fertilizers. We demonstrate the approach through simulation. Based on our previous observations of variation in P and K from four fields in Cambridgeshire, England, we generated 100 realizations of P and K in each field using geostatistical simulation. We did so with various combinations of sizes of total sample and calibration set. For each such sample we assigned various proportions for calibration on which notionally both soil spectroscopy and chemical concentrations were determined. Knowing the costs for labour in the field for sampling, the preparation of soil in the laboratory, the spectroscopy, chemical analysis and amortization of equipment, we estimated the costs of acquiring data. Set against these were the costs of error, i.e. of uncertainty, in the final predictions by kriging arising from calibration error and spatial variation. For each combination we computed the fertilizer required to minimize the expected loss associated with predictions, where the expected loss is the difference in profit between applying fertilizer for the estimated concentrations of P and K and their true concentrations. The size of the calibration set outweighed the effect of total sample size on the uncertainty associated with predictions. Equally, for the same size of calibration set, there were large differences in the kriging variances between total sample sizes. When the costs of acquiring data were disregarded, the expected loss for available P was strongly affected by the total sample size. For available K, the effect of the size of the calibration sample dominated the expected loss. The expected loss showed diminishing returns with increasing sample size. None of the sample sizes considered would result in a financial gain: spectroscopy needs to become cheaper for it to be cost-effective for variable-rate applications of P and K fertilizer.

1. Introduction

Modern farmers are keen to vary their application of fertilizer in accord with the spatial variation of plant nutrients in the soil within individual fields. They or their advisers cannot measure the nutrient concentrations everywhere, however: they must rely on measurements from finite numbers of locations, which may then be used to estimate the concentrations everywhere else by some form of interpolation. Kriging is now well-established as best practice for the interpolation; it provides unbiased predictions with minimal error variances, which themselves are estimated. A kriged prediction is a weighted average of observed values for a variable with weights determined from a model of spatial covariance. That model must also be obtained from sample data, and we know from a great deal of experience that samples of 100 or more are required for reliable models, though this number depends to some extent on the underlying complexity of the soil variation and its geographical scale (Webster and Oliver, 1992; Lark, 2000). Given the costs and time expenditure of traditional soil analyses, the number of samples required for kriging is often impractical.

One way to cut costs is to replace the traditional methods of soil analysis by cheaper spectroscopy of soil samples, either in the laboratory or in the field. There have been much research and many successful applications of spectroscopy to determine chemical, physical and biological properties of soil (Guerrero et al., 2010; Viscarra Rossel et al., 2022). They are motivated not only by spectroscopy's being

* Correspondence to: Joint Research Centre (JRC), Ispra 21027, Italy.
E-mail address: timo.breure@ec.europa.eu (T.S. Breure).

https://doi.org/10.1016/j.geoderma.2025.117504
Received 4 April 2025; Received in revised form 1 September 2025; Accepted 4 September 2025
Available online 6 October 2025

cheaper than traditional laboratory methods but also because it is non-destructive (in the case of *in-situ* measurements), requires no hazardous chemicals and can predict multiple soil properties from a single measurement (Viscarra Rossel et al., 2006). Spectroscopy enables one to predict soil properties in a cost-effective way, to process more samples than by traditional methods and thereby to obtain more information about the soil and its variation.

To predict a soil property by spectroscopy the spectra must be calibrated. The spectra of representative subsets of samples are related to the measurements obtained by wet chemical analysis on representative subsets of samples by statistical models (known as the calibration models and typically some form of regression). The calibration models are then used to predict the values for all members of the population of interest. Such a model is subject to uncertainty, however, and it can be biased. For both accurate and precise predictions, a calibration set that covers the ranges of the properties concerned is essential (Viscarra Rossel et al., 2011; Schmidt et al., 2014). Otherwise the models obtained are likely to be unstable and lead to biased estimates (Bellon-Maurel and McBratney, 2011). In general, the more samples of soil used for calibration the less will be the uncertainty of predictions, though the cost will be greater.

The two sources of uncertainty described above (kriging error and calibration error) can usually be reduced by an increase in sampling. The kriging error can be reduced by denser sampling. The calibration error can be reduced by an increase in the size of the calibration sample. The sampling itself constitutes a large part of the cost of a survey by soil spectroscopy in addition to the cost of the chemical analysis of the calibration samples (de Gruijter et al., 2018). According to Viscarra Rossel et al. (2011), most of the published literature on soil spectroscopy considers sampling designs of either geographical space or feature space but not both. Exceptions are the papers by Minasny et al. (2007), de Gruijter et al. (2010, 2018), Adamchuk et al. (2008, 2011), Shaw et al. (2016) and Behrens et al. (2024). Of these only de Gruijter et al. (2018) and Shaw et al. (2016) take into account the value of reducing uncertainty against the costs of sampling.

The notion of setting the cost against the accuracy of survey is not new: Yates (1981), in the first edition of his book published in 1949, provided an equation relating the expected loss in accuracy to the sampling effort. This equation allows one to determine the sampling effort required to minimize the expected financial loss arising from the sampling. It is referred to as an 'expectation' because the estimate itself has an associated probability distribution. Lark and Knights (2015) developed concept. They described the expected loss by a function for the costs incurred from decisions based on an estimated value, given its deviation from the true value. They noted that in general the loss function is asymmetric because the consequences of over- and under-estimation differ in kind and magnitude. Depending on the loss function's asymmetry, there might be a slight preference towards either over- or under-estimation. Consequently, the optimum value might not be equivalent to the largest expected financial gain.

Our aim is to develop a loss-function framework to explore how sizes of sample sets and calibration sets affect the likely profitability of variable-rate applications of P and K fertilizers based on soil spectral predictions, and to demonstrate this approach. To quantify the expected losses associated with using uncertain information, we must know the true underlying variation of the plant nutrients in the fields. This is not feasible in practice, and so we turn to *in-silico* experiment. Firstly, we simulate the underlying variation in the fields, by geostatistical simulation. This method is used to generate multiple, equally probable spatial representations (or realizations) of a variable based on limited sample data and statistical models of spatial continuity (e.g. variograms). For each realization, we then simulate the process of sampling in those fields and the subsequent decision making about variable-rate fertilizer application. We consider two possible financial losses in this context: (1) the loss in crop yield because too little fertilizer is applied and (2) the unnecessary cost of applying too much fertilizer. We quantify the uncertainty in the estimates of available P and K from spectra for several sizes of calibration samples and total samples for mapping. We then investigate the effect of this uncertainty on decision-making for fertilizer application within the framework of the loss function. We aimed to answer the following questions.

- How does total sample size and total number of calibration samples affect prediction accuracy?
- How does total sample size and total number of calibration samples affect expected loss when sampling costs are not accounted for?
- How does total sample size and total number of calibration samples affect expected profit when sampling costs are accounted for?

2. Methods

We aimed to simulate the process of sampling across a field to predict the soil properties from spectral measurements. In summary, our procedure was a follows. First, we took data on spectroscopic and analytical measurements of P and K from several fields in the Fen district of the UK (Breure et al., 2021, 2022), and estimated covariance structures (Fig. 1a). Based on these covariance structures, we simulated random realizations of the variation in nutrients in our in-silico fields (Fig. 1b). We then selected a subset of size N_t from each realization as if we were sampling an actual field. We then chose a subsample from the N_t of size n_c as a calibration set. For each calibration there is an error which we assume to be normally distributed (Fig. 1c). We sampled from this distribution and added this error to the P and K values (Fig. 1d). Having simulated the acquisition of the concentrations of P and K, we predicted the spatial variation in P and K from punctual spectral measurements to guide fertilizer management (Fig. 1e). We then used dose–response curves to calculate the amount of fertilizer to apply, both on the prediction (F_0) and the prediction and its variance (F_{opt}) (Fig. 1f). We quantified the expected loss due to applying fertilizer from spectroscopy estimates compared with the theoretical optimum fertilizer (based on the true P and K concentrations as simulated) (Fig. 1 g). We then subtracted the expected profit associated with precise fertilizer application from spectroscopy estimates with the costs of the data acquisition (Fig. 1h).

2.1. Study area, sampling, wet chemistry analysis and spectroscopy

Our study is based on data obtained in sample surveys of three fields in the Fen district of Cambridgeshire, England, in 2018 and 2019 (Breure et al., 2021). The region was originally dominated by peat, much of which has oxidized since the land was drained in the 17th century. Now the underlying alluvial and marine deposits have become exposed revealing complex patterns of soil variation within fields (Hodge et al., 1984).

To characterize the variation in P and K we took soil samples from across each field. Breure et al. (2021) describe in detail the sampling designs, the wet chemical analysis, the spectroscopy and the calibration. Here we summarize them briefly. The sampling design of Field 1 (8.2 ha) was based around a 30-m square grid, with three transects (on alternate rows of the grid) more intensely sampled at 6-m intervals. The designs for Field 2 (16.9 ha), Field 3 (5.1 ha) and Field 4 (8.9 ha) were computed by spatial coverage sampling (Walvoort et al., 2010). From these initial points we selected a subset with balanced sampling (Grafström and Lisic, 2019) on the spatial coordinates and elevation (measured by LiDAR). The number of samples in this subset was 36 for Field 2 and 32 for Field 3. At each location of these subsamples, we added another sampling point 6 m away at a random orientation to estimate the short-range spatial variance.

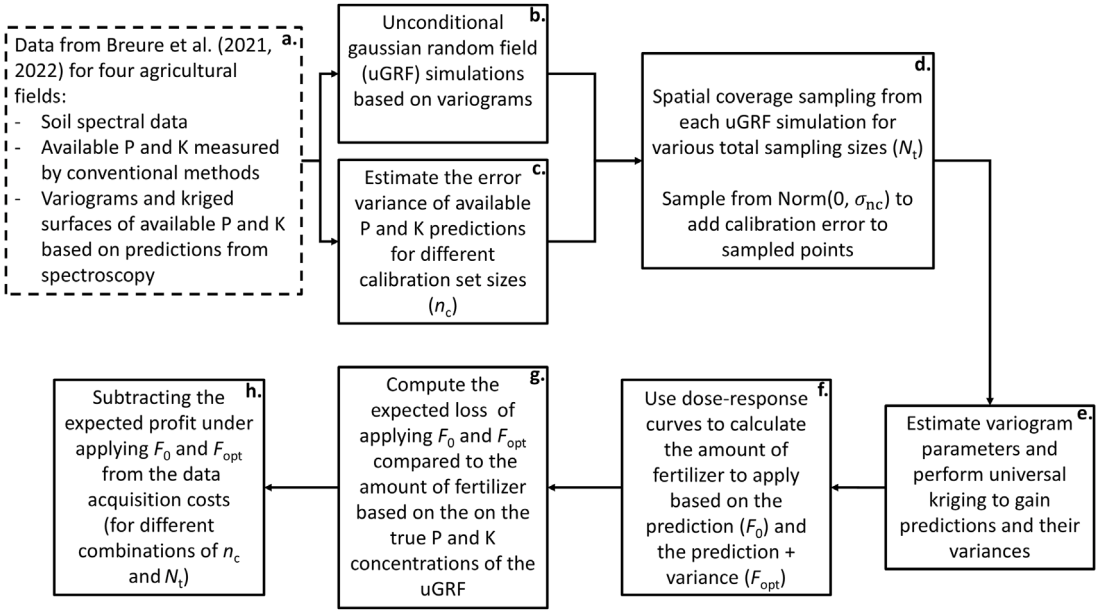

Fig. 1. Flow chart that specifies the data source and various methodological steps.

Spectra were taken on each of the soil samples. They comprised near-infrared (NIR) and mid-infrared (MIR) measurements with a Tensor II spectrometer (Bruker, Ettlingen, Germany), and X-ray fluorescence (XRF) spectra, measured by a DP-6000 Delta Premium portable X-ray fluorescence (pXRF) spectrometer (Olympus Ltd, Center Valley, USA). Available P and K do not have direct absorption features in the NIR region. In the MIR region, phosphates show distinct absorption bands related to the phosphate group, specifically around 1100–1000 cm^{-1} (P–O stretching) and 600–500 cm^{-1} (bending modes). However, available P and K can be predicted to some extent due to their relationship to other soil components that have distinct absorption features in the NIR and MIR region, such as clay minerals (Soriano-Disla et al., 2013). In the XRF region, potassium exhibits emission lines at 3.31 keV and 3.59 keV, and phosphorus at approximately 2.01 keV and 2.14 keV. These emission lines refer to the total element concentrations but can be calibrated to available nutrient content (Breure et al., 2022). The pXRF samples where measured in three replicates of each soil sample, near- and mid-infrared spectra were measured on three replicate subsamples of each soil sample. Further analysis was done on the mean spectra of the three measurements. The raw spectra were pre-processed with a Savitzky–Golay filter (Savitzky and Golay, 1964) and then transformed to their first derivatives. To predict a variable from soil spectra, we developed a calibration model by regression of the spectra (using partial least squares regression) on wet chemistry measurements made on a subset of the soil cores (for details see Breure et al., 2021). In each field we selected 30 locations to be measured by wet chemistry using a balanced sampling approach on the coordinates and elevation (from LiDAR). These samples measured by wet chemistry comprised our calibration set ($n = 120$).

2.2. Geostatistics of available P and K

The nutrient predictions from spectroscopy were then used to interpolate available P and K across the fields, see Breure et al. (2021) for a detailed description. Briefly, we fitted a linear mixed model to the data with the trend factors as fixed effects and the spatial autocorrelation captured in the random term (see Lark and Cullis, 2004). The autocorrelation in the random term seemed to be well described by either an exponential or spherical variogram, one of which had to be selected *a priori*. We compared the two by log-likelihood ratio testing.

Table 1
Fixed effects and parameters estimated by REML of the exponential variograms, L stands for LiDAR (elevation), and x_1 and x_2 are the spatial coordinates. The variogram parameters are the nugget variance (c_0) the sill (c_1) and the range (a) respectively.

Field	Soil property	Fixed effects	Variogram parameters		
			c_0	c_1	a
1	P/mg kg^{-1}	x_1, x_2, x_1^2, x_2^2, x_1x_2	17	67	50
	K/mg kg^{-1}	x_1, x_2, x_1^2, x_2^2, x_1x_2	2930	1942	40
2	P/mg kg^{-1}	L, x_1, x_2	13	57	39
	K/mg kg^{-1}	L, x_1, x_2	3337	4917	32
3	P/mg kg^{-1}	L, x_1, x_2, x_1^2, x_2^2, x_1x_2	22	40	30
	log(K/mg kg^{-1})	L, x_1, x_2, x_1^2, x_2^2, x_1x_2	0.023	0.097	6.62
4	P/mg kg^{-1}	L	30	125	14
	K/mg kg^{-1}	x_1, x_2, x_1^2, x_2^2, x_1x_2	260	2473	12

To test the significance of the coordinates (eastings, northings and an interaction term) and elevation as trend parameters, we added each in turn and did a log-likelihood ratio-test. We fitted models for the variograms by Maximum Likelihood to allow for the comparison between models with a different number of fixed effect parameters. A chi-squared p-value of 0.05 from the log-likelihood ratio was taken as significant evidence that the trend parameters should be included. Once we had chosen a final set of fixed effects, both the fixed and random effects (variogram parameters) were estimated by residual maximum likelihood (REML). Statisticians generally prefer REML because it reduces bias in the random effect parameters caused by uncertainty in the fixed effect parameters Lark et al., 2006. The estimates of the random- and fixed-effect parameters are listed in Table 1.

To produce simulated fields we approximated more realistic variations of available P and K by simulating unconditional Gaussian random fields (uGRFs). As we were concerned with simulating variations of P and K that could be feasibly found in agricultural fields, but not specifically the ones we had physically sampled, we did not condition the simulations on the measured data (see Webster and Oliver, 2007). Thus, for simulating uGRFs, we had to characterize the covariance structure in each field, which were based on the variogram parameters listed in Table 1. To comply with computational limitations we resampled the rasters from Breure et al. (2022) to a raster cell resolution of 4 m × 4 m. We used Cholesky decomposition to define the square root of the

covariance matrix. We restricted the uGRFs to positive values by re-simulating grid cells if the values were less than or equal to 0. We simulated 100 uGRFs for each field. We considered these simulated data the underlying true available P and K values, denoted S, at given locations.

2.3. Estimating the error from the calibration regression for different numbers of calibration samples

To quantify the uncertainties related to the calibration we formulated an equation that described the prediction error variance as a function of the number of calibration samples (n_c). We followed the same methodology as in Breure et al. (2022) for calibration. Given that we had rather few samples within each field with wet chemistry data, we pooled samples for all four fields for calibration. The pooled set ($n = 120$) was used to select calibration samples by the conventional method for the Kennard–Stone algorithm on a matrix of combined NIR, MIR and XRF soil spectra. This method allows one to select samples with a uniform distribution over the predictor space based on their Euclidean distances (Kennard and Stone, 1969). The number of calibration samples varied from 15 to 75% of the samples. The minimum calibration set size considered was 18 samples, given that we evaluated a maximum of 15 components in the partial least squares regression; see Breure et al. (2022) for further details. We used the calibration dataset for predicting the remaining validation set. For each bootstrap simulation we computed the mean-squared error (MSE), and the average MSE was used as an accuracy metric to describe the error variance, denoted by $\sigma^2_{n_c}$, where n_c stands for the number of samples in the calibration set.

2.4. Procedure to compute kriging predictions for different sample sizes from in-silico fields

We selected sampling points for spectral measurements of P and K in the field. For this we computed a spatial coverage sampling design for N_t samples. A spatial coverage design allows sample locations to be evenly spread across the domain of interest to minimize the maximum interpolation error (Webster and Oliver, 2007). To obtain robust estimates of the variation at shorter distances one should sample at locations closer apart than the maximum range at which the variable is spatially correlated. We therefore selected a subset of 20 locations by balanced sampling on the eastings, northings and LiDAR and an additional sample point added 6 m away from each in a random direction. At each *in-silico* sample location we assumed that the variable is predicted from spectroscopy. To account for the associated calibration error, we sampled from the normal distribution Norm(0, σ_{n_c}) and added that to the simulated true value of the soil to give our observed predicted value. These observed values were then kriged as follows.

Visual inspection is unsuitable for the number of variograms to be estimated within our analysis ($n = 800$). We therefore took the following approach to obtain initial estimates of the parameters for an exponential variogram. First, we took the outermost locations of the spatial coverage sampling design as the bounding box (i.e. approximating the boundaries of the agricultural field). The initial estimate of the distance parameter (a) was one tenth of the diagonal of the bounding box. We used half the diagonal as the maximum distance for the experimental variogram. Second, we computed the omnidirectional sample variogram using the method of moments (Webster and Oliver, 2007). The minimum of the experimental variogram's semivariance was taken as the initial estimate for the nugget parameter (c_0). The mean value of the median and maximum semivariance was used as the initial estimate of the sill parameter (c_1). The variogram parameters were then estimated by REML. Where the estimated nugget parameter was less than the known error from calibration, $\sigma^2_{n_c}$ the model was refitted with $c_0 = \sigma^2_{n_c}$; similarly c_0 was restricted so as not to be less than zero. The variogram model was then used for ordinary punctual kriging. Once we obtained the kriging predictions and their error variances at each location, we added back the trend to the predictions.

2.5. The loss function and variable costs of the data acquisition

We quantified the effect of error in the estimates of P and K by a loss function, $L(F, S)$, for a given application of fertilizer, F, which is defined as the difference in profit that results from applying a given amount of fertilizer F compared with an economically optimal amount of fertilizer F_0:

$$L(F, S) = \Phi(F_0) - \Phi(F) , \tag{1}$$

where the profit $\Phi(F)$ is the difference between the income from the crop (price of the crop × yield) and the cost of the fertilizer:

$$\Phi(F) = M \times \text{Yield} - V \times F , \tag{2}$$

where M is the price of the crop (in £ t^{-1}) and V is the cost of the fertilizer (in £ kg^{-1}).

Given our focus on precise fertilizer application, we assume that the yield is given by the dose–response equation:

$$\text{Yield} = \alpha + \eta R^{\xi F + S} + \nu(\xi F + S) , \tag{3}$$

where S is the concentration of the nutrient in the soil, F is the applied fertilizer (kg ha^{-1}), ξ is the increase in nutrient concentration (mg kg^{-1}) in the soil for every 1 kg ha^{-1} fertilizer applied, and α, η, ν and R are parameters. Eq. (3) describes the generic dose–response curve function. The fields from our study were used to grow lettuce, and so we derived relevant dose–response curves from the literature for both P and K for this crop (Greenwood et al., 1980; Prasad et al., 1988). See Supplementary Fig. 1 for the fitted models, as used in Breure et al. (2022). We assumed that for every 1 kg of P added in fertilizer 0.18 kg becomes available to the crop (Muhammed et al., 2017), for every 1 kg of K added in fertilizer, 0.62 kg becomes available to the crop (Blake et al., 1999). Furthermore, we assumed that the added nutrients are contained in the top 25 cm of the soil (the sampling depth). We took from Milne et al. (2006) the value of 480 kg m^{-3} for bulk density of this peat soil. Given the support of our kriged predictions (4 m × 4 m), it follows that an addition of 1 kg fertilizer per ha leads to an increase in the concentration of this layer of 0.15 mg available P kg^{-1} and 0.52 mg available K kg^{-1}, equal to ξ in the dose–response Eq. (3). Greenwood et al. (1980) listed a mean base nutrient concentration of 69 mg available K kg^{-1} for the unfertilized soil in their study, which was used as an additive component. We assumed a profit margin (M) of £90 per tonne of lettuce. The prices of fertilizer (V) were taken as £0.36 per kg P fertilizer and £0.29 per kg K fertilizer.

We then calculated, from Eq. (2), the economically optimum amount of fertilizer, which is given by:

$$F_0 = \ln\left(\frac{B/\xi - \nu}{\eta R^S \ln R}\right) / \xi \ln R , \tag{4}$$

where $B = V/M$, known as the break-even ratio. By definition, the loss given by Eq. (1) is zero when the optimum amount of fertilizer is applied. However, computing the optimum amount of fertilizer to apply relies on an exact estimate $\hat{S}$, whereas predictions from kriging have an associated error distribution, described by $g(S, \sigma_s)$, where σ_s equals the kriging variance. Given the error distribution, we computed the optimum fertilizer rate that maximizes the expected profit:

$$F_{\text{opt}} = \ln\left(\frac{B/\xi - \nu}{\eta \ln R \int_0^\infty R^S g(S, \sigma_s) \mathrm{d}S}\right) / \xi \ln R . \tag{5}$$

The application of F_{opt} minimizes the expected loss function, $\mathrm{E}[L(F, \hat{S})]$, which we define here as the difference between the profit where S is known without error and the profit under the fertilizer application based on the kriged soil nutrient value, $\hat{S}$.

$$\mathrm{E}[L(F, \hat{S})] = \Phi(F_0) - \Phi(F, \hat{S}) . \tag{6}$$

We computed $\mathrm{E}[L(F, \hat{S})]$ for two scenarios. One where the fertilizer regime, F given $\hat{S}$ equals the application of F_0, Eq. (4) and the second

Table 2
The costs associated with soil sampling in the field, spectroscopy and chemical analysis.

Activity	Cost per sample/£
Field sampling	5.70
Sample processing and spectrometry	5.50
Sample preprocessing for wet chemistry	3.38
Wet chemical analysis for available K	14.70
Wet chemical analysis for available P	16.30

where we account for the uncertainty in our estimate of $\hat{S}$, and F equals the application of F_{opt}, Eq. (5).

The major constraints to accurate predictions are the costs of spectroscopy at the field scale. These include the costs of sieving, milling, weighing, wet chemistry for calibration and spectroscopy of the soil samples plus the sampling campaign itself. The costs of the total number of samples, N_t, and the number of samples used in calibration, n_c, were approximated as a simple linear function formulated by the costs of field sampling, spectroscopy, sample processing, sample handling and analytical measurements:

$$C(N_t, n_c) = \Omega N_t + \delta n_c \ . \tag{7}$$

Table 2 summarizes the costs associated with the five main steps of data acquisition. They include sampling in the field at £5.70 per sample. The costs of spectroscopy consist of both milling and loading sample plates for the bench-top spectrometer at a rate of 60 samples for one full working day of a technician, and are included in the costs for the total number of samples (Ω). Based on a salary of £135 per day this would be equivalent to £2.25 per sample. Given that the XRF spectrometry is a separate procedure, we doubled this value to £5.50. The costs associated with n_c were approximated as a function of the sample handling (sieving and weighing) and the wet chemistry costs, denoted as δ. Based on our experience of laboratory procedure, we assumed that sieving and weighing would take 20 min per sample (one working day for 40 samples to sieve and weigh), equivalent to £3.38 per sample. The costs, again based on those in our laboratory at the time, of analysing available K by ammonium-nitrate extraction and ICP-OES was estimated at £14.70 per sample. The analysis for available P by the Olsen method was estimated at £16.30 per sample. These prices were based on those of the analytical laboratory at Rothamsted Research at the time of analysis (2018–2019).

We expected that the sampling costs would exert a strong influence on the expected profit. We therefore applied a scaling factor to the costs of data acquisition, $C(N_t, n_c)$, to explore the degree to which sampling costs would need to diminish to make variable-rate fertilizer supported by spectroscopy financially viable. We iteratively applied a scaling factor to assess its effect on the expected profit. Based on this, we applied a scaling factor of 5%, 1% and 0.5% of the original costs of data acquisition.

3. Software

Analysis was done with base R commands and the following R packages as implemented in RStudio: data handling with the **sf** and **tidyverse** packages (Pebesma, 2018; Wickham et al., 2019), computation of the sampling designs using the **spcosa** (Walvoort et al., 2010), **BalancedSampling** (Grafström and Lisic, 2019) and **SpatialEco** (Evans, 2019) packages, spectral processing using **prospectr** (Stevens and Ramirez-Lopez, 2013), partial least squares regression using **pls** (Bjørn-Helge et al., 2019), Granger–Ramanathan averaging with **GeomComb** (Weiss and Roetzer, 2016), model-based geostatistics with the **geoR** and **georob** packages (Ribeiro and Diggle, 2018; (Papritz, 2025)) and handling of spatial objects with the **raster** (Hijmans, 2020) and **rgdal** (Bivand et al., 2020) packages. Graphics were created with base R and the package **ggplot2** (Wickham, 2016).

Table 3
Parameters for the exponential equation that describes the error variance $\sigma^2_{n_c}$ as a function of the number of calibration samples (n_c) used in regression.

Soil property	A	b	ω
Available P	3	1893	0.765
Available K	63	192 211	0.768

4. Results

4.1. Error variance as a function of the number of calibration samples

Based on the partial-least squares regression and its bootstrapped estimates, the relationship between the number of calibration samples and the associated error variance was described by a simple exponential function:

$$\sigma^2_{n_c} = A + b\omega^{n_c} \ , \tag{8}$$

where n_c is the number of calibration samples used for the regression, and A, b and ω are model parameters.

For both available P and K the function reaches its asymptote after around 40 calibration samples. This function indicates a limit on the accuracy with which available P and K can be predicted (Fig. 2). Based on these results, we decided to test for the range in n_c of 20 to 40 in steps of 5 in further steps in the analysis.

The estimated parameters for the exponential equations are given in Table 3.

4.2. Prediction uncertainty under several sample sizes

The kriging variance depends on sampling configuration and density, and it follows that increasing the density (and number) of samples should reduce the kriging variance. As expected for both available P and K, an increase in the number of calibration samples (n_c) was accompanied by a decrease in the median kriging variance (Fig. 3). For the total sample size (N_t) there was a similar trend in the kriging variance. For a given value of n_c, the kriging variance is more accurately estimated once N_t increases (there is less spread in the box-plots). The exception is available P for Field 4, where more often a pure nugget variogram was fitted.

Like the kriging variance, the estimated nugget parameter decreases as n_c increases. The nugget variance as a function of N_t exhibits different behaviour, however. For both P and K and across all fields, the variance of the estimated nugget parameter diminishes as the total sample size increases (N_t). That is, the distance between the 1st and 3rd quantile in the box-plots narrows (see Fig. 4).

4.3. Expected loss without accounting for data acquisition costs

The mean expected loss (E[$L(F_{\text{opt}})$] / £ ha^{-1}) decreased with increase in sample size for Fields 1, 2 and 3, but the difference was significant only for P in Field 2. Even then, the relative changes in expected loss are small. There was no clear effect of the size of the calibration set, n_c (Fig. 5).

Within our computation of (E[$L(F_{\text{opt}})$]) we accounted for the uncertainty in the soil estimates. The probability distribution described by the kriging variance is integrated within the denominator of Eq. (5) to compute the optimum amount of fertilizer under uncertainty. Generally, accounting for uncertainty reduced the expected loss (compared with E[$L(F_0)$]), although the effect was small (Supplementary Fig. 1). Furthermore, it shows that there is substantial variation between the simulations. For a given combination of N_t and n_c the box-plot values can be either positive or negative. This seems to depend on how well the spatial variation is characterized and thus how informative the uncertainty is. For example, for available P in Field 4 the uncertainty is unhelpful and leads to a larger expected loss (Supplementary Fig. 2).

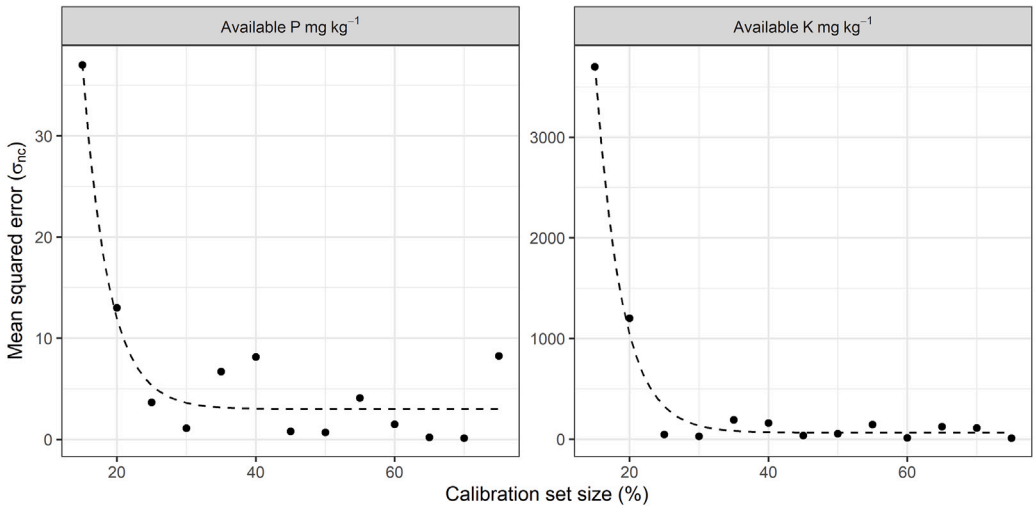

Fig. 2. Parameters for the exponential equation that describes the error variance $\sigma^2_{n_c}$ as a function of the number of calibration samples (n_c) used in regression.

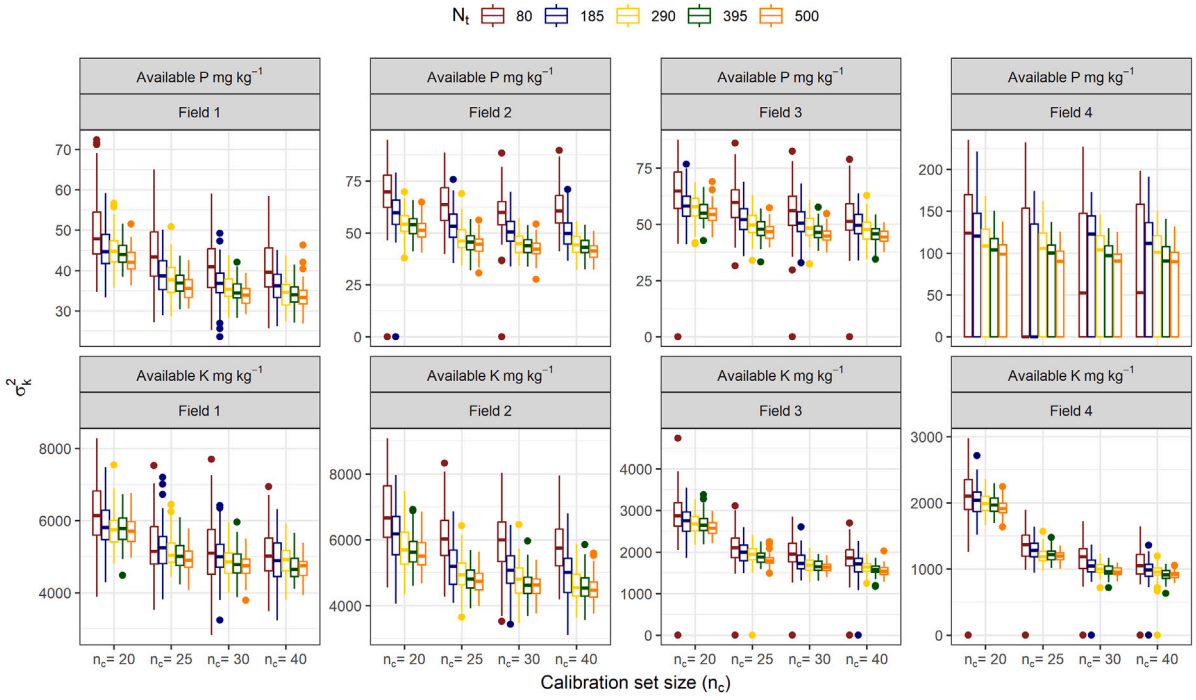

Fig. 3. Kriging variance (σ^2_k) distributions for the in-silico simulation results as a function of total sample size (N_t) and calibration sample size (n_c).

4.4. Expected profit when data acquisition costs are taken into account

For each field, the expected profit ($\Phi(F_{opt})$/£ ha^{-1}) from P and K fertilizer declines linearly as the size of sample increases (Fig. 6). The linear relation shows that the sampling costs predominate, Eq. (7), over the potential increases in profit based on the non-linear dose–response curve, Eq. (3). The slopes differ between fields because the overall sampling costs are spread over different areas (Field 2 is larger than Field 3). There is no variation in the expected profit as a function of different calibration set sizes, indicating that these make up a relatively small amount of the costs.

The last step in our analysis was to apply a scaling factor to the costs of data acquisition of both total and calibration sample size, Eq. (7), to discover the cost at which implementation of spectroscopy would become financially viable. Fig. 7 shows the result in which the distribution of $\Phi(F_{opt})$ over the range of n_c is plotted against total sample size (N_t). The results showed that for available P and K across all fields the cost of data acquisition would have to be less than 5% of their assumed value (Table 2) to eliminate the decline in, $\Phi(F_{opt})$, as function of N_t. However, in the scenario of 0.5% of the current data acquisition costs, $C(N_t, n_c)$, sampling by spectroscopy leads to an increase in expected profit in only two cases, namely for available P in Field 2 and Field 4 (Fig. 7). In all other cases, the expected profit stabilized as a function of N_t but did not lead to an increase. Last, we note that the ordinate in Fig. 7 does not start at 0, and indeed the effect of sampling on the expected profit is marginal.

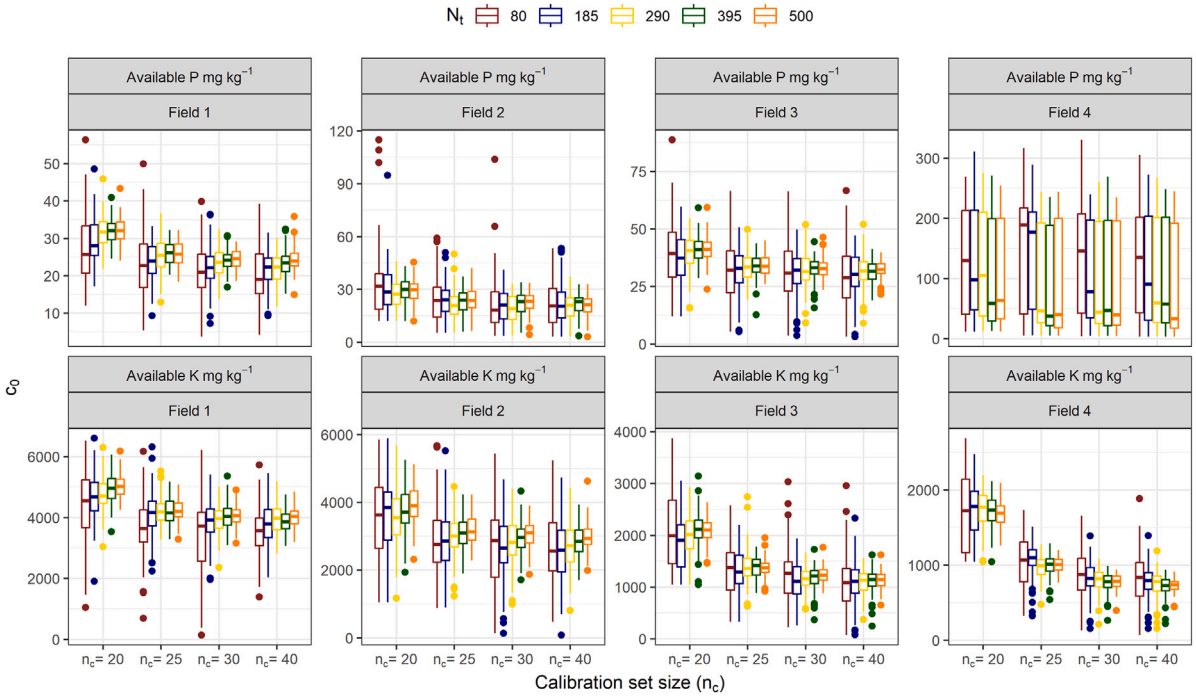

Fig. 4. Nugget variance (c_0) distributions for the in-silico simulation results as a function of total sample size (N_t) and calibration sample size (n_c).

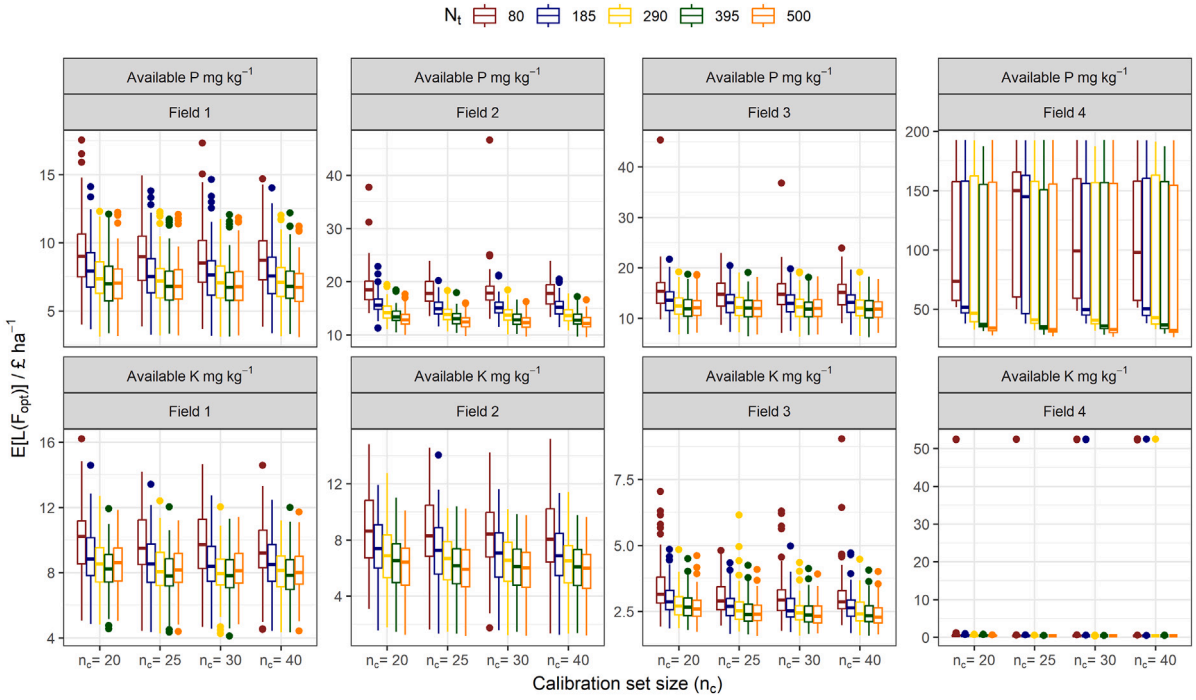

Fig. 5. Expected loss, E[$L(F_{opt})$], distributions for the in-silico simulation results as a function of total sample size (N_t) and calibration sample size (n_c).

5. Discussion

5.1. Uncertainty in soil properties predicted from spectroscopy at the field-scale

Our analysis showed that the number of calibration samples has a large effect on the kriging variance. In some cases, the kriging variance was less sensitive to total sample size for the range of sample sizes we selected. These findings contrast with those of Brodský et al. (2013) and Viscarra Rossel et al. (2016) who found the contribution of the errors from the spectroscopic modelling to be smaller than those from the spatial variation. Those results were for the prediction of soil organic carbon, which has distinct spectral features in the infrared region of the spectrum (Kuang et al., 2012) unlike those for available P and K (except for the total P and K content measured by XRF). Ramirez-Lopez et al. (2019) propagated the calibration error through in their mapping of particle-size fractions and exchangeable calcium content and showed that the contribution of the calibration error variance was relatively

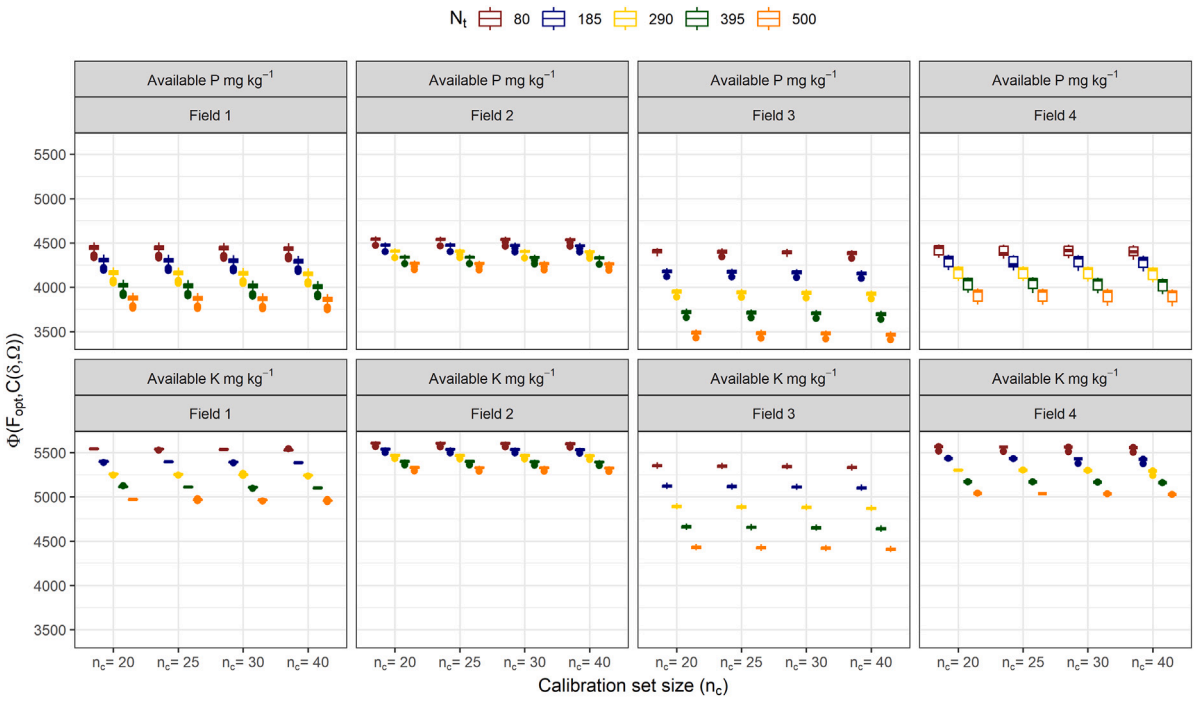

Fig. 6. Expected profit, $\Phi(F_{opt})$, distributions for the in-silico simulation results as a function of total sample size (N_t) and calibration sample size (n_c).

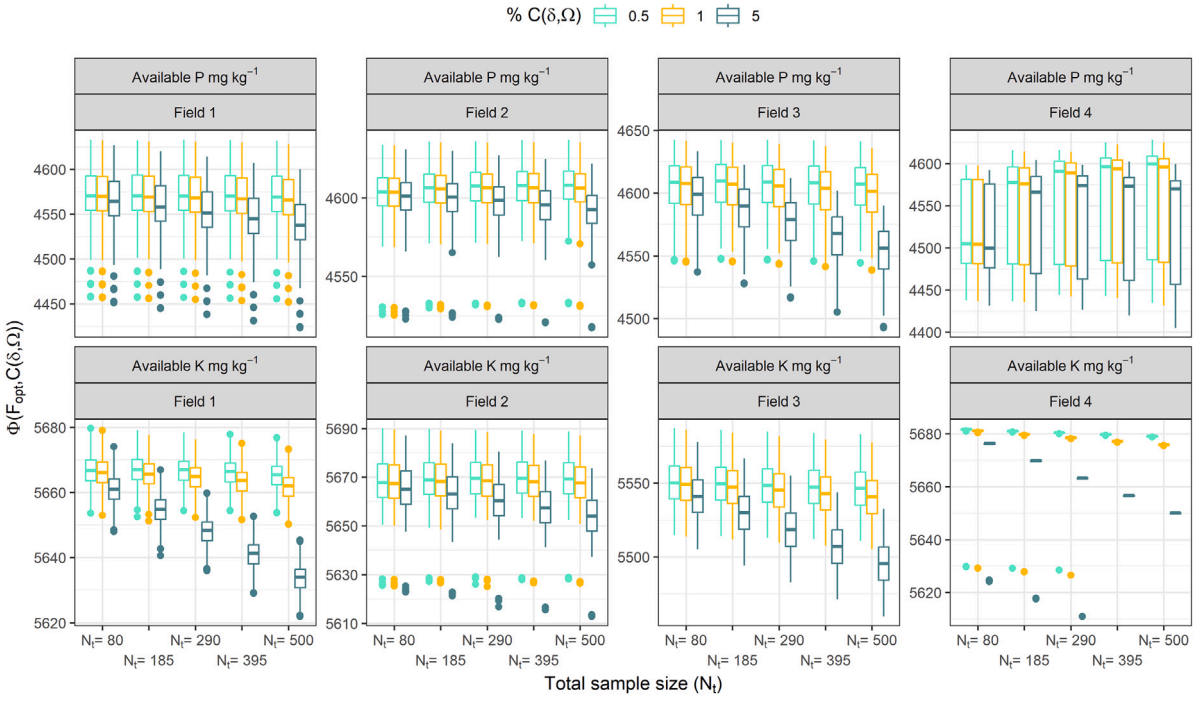

Fig. 7. Expected profit, $\Phi(F_{opt})$, distributions for the in-silico simulation results as a function of total sample size (N_t) over the range of calibration sample size (n_c). Colours indicate the scaling factor applied to the costs of data acquisition, $C(N_t, n_c)$, given in % of the original data acquisition costs.

large, leading to enhanced smoothing of the kriging predictions as a result of the large nugget variance.

The relation between uncertainty introduced by the calibration error and the spatial uncertainty is likely to depend on the underlying soil variation and the number of samples considered. We considered a range in total sample size from 100 (and more) because this number is generally considered the minimum required for reliable estimation of the variogram. Across varying numbers N_t, sampling designs included a fixed number of close points ($n = 20$). These ensure that the spatial covariance parameters are well estimated (Lark and Marchant, 2018; Wadoux et al., 2019). Depending on the nugget variance of the original variogram (Table 1), the effect of total sample-size on the nugget variance was smaller for larger values of N_t. We attribute this to the estimated nugget variance's being close to the true underlying short-scale variance. These results accord with expectations: larger sample sizes generally lead to more accurate estimates of short-range variation.

Another consideration regarding the total sample size is its effect on estimating the underlying trend. The total sample size was computed

by a spatial coverage design that leads to accurate estimation of the trend parameters (Brus et al., 2019). Since we removed the trend surface prior to 'sampling', the effect of the total sample size on the trend estimation has been ignored. In an actual soil survey, however, differences in estimation of the trend have a large effect on subsequent kriging predictions and the representation of associated uncertainty (Lark, 2009). Consequently, we should expect the effect of different total sample sizes on the expected loss to be larger as the trend surface is approximated with increasing accuracy.

For our study, we simulated unconditional Gaussian random fields (uGRFs) to obtain variations of available P and K for our target fields. The uGRFs were used as a technique to simulate the underlying spatial variation of the nutrients so that we could explore losses compared with having perfect information. While we demonstrate our approach through simulation it has immediate practical relevance. Data from reconnaissance surveys or (more likely) the literature can be used to estimate calibration and kriging errors thereby allowing analysts to estimate the likely profitability of variable rate management under various sampling strategies and so make informed decisions about sampling and application of fertilizer at variable rates.

5.2. Expected losses from informing fertilizer application on spectroscopic estimates

Overall, the results of the expected loss show that soil spectroscopy could provide sufficiently accurate estimates of available P and K for predicting fertilizer requirement. The expected losses, compared with the theoretical optimum, ranged from £4.2 to 30 ha^{-1} for P and £0.4 to 17.9 ha^{-1} for K. These values are negligible compared with the average profit per hectare and pose little risk to the grower. Furthermore, for both P and K there were diminishing returns on investment for increased sample sizes, indicating that there will be an optimum number for both total and calibration samples. Note, however, that the magnitude of the expected loss and resulting calculated optimum are determined by the formulation of the loss function. For example, the true values for available K in fields 1 and 2 were generally above the asymptote of the dose–response curve (Supplementary Fig. 1). Consequently, omitting fertilizer application for large parts of the field resulted in the largest financial gain. Equally, the asymmetry in the loss function might explain the contrast in the expected loss between F_0 and F_{opt} (Supplementary Fig. 1). Given the asymptote in the dose–response curve for K fertilizer, risk-averse over-application of fertilizer under uncertainty leads to a greater expected loss.

5.3. How cost-effective is spectroscopy at the field-scale?

Our results show that under current costs of data acquisition including the sampling procedure, the implementation of spectroscopy was not cost-effective. These findings were supported by a linear decrease in expected profit for large total sample sizes (N_t). For soil spectroscopy to become cost-effective, the current costs need to diminish by at least 95%. One could pursue this kind of investigation within the framework of a loss function for different configurations of sensors (e.g. only MIR and XRF) or take *in-situ* spectral measurements to reduce the costs of data acquisition. In the situations we investigated, however, for the fields we sampled with their particular variation in P and K and our configuration of sensors costs would have to be reduced to make the whole procedure worthwhile for farmers.

Breure et al. (2022) explored the expected loss associated with variable-rate precise and uniform blanket fertilizer application of P and K for the same fields as those in this study. They concluded that the difference in the expected loss between these two fertilizer regimes could indicate the allowable expense for a field survey. The differences in expected loss between these two regimes lay in the range £15–47 ha^{-1} for available P. The differences in the expected loss for available K lay in the range £0–15 ha^{-1}. Given Eq. (7), the least sampling costs in this study are £49 ha^{-1} for P and £47 ha^{-1} for K. These values are approximately equal to the differences in expected loss between variable-rate and uniform applications of P. However, the smallest sampling cost (£49) is based on Field 2, which is almost twice the size of Field 4, which showed a difference of £47 ha^{-1} between the two fertilizer regimes.

Our findings hold true under the current assumptions of prices, data acquisition costs and the formulation of the loss function. Further studies are required to elaborate on these assumptions. For example, we did not consider a scaling effect of the sampling costs per sample relative to the total sample size. Within a larger geographical area, the variable costs per sample will scale with an increase in total sample size due to reduced travel-time between locations (Lark and Knights, 2015). Equally, the economy of scale might be applicable to the number of samples analysed by wet chemistry. That is, for a larger number of samples a laboratory might charge a lower price per sample. Our results showed a marked decrease in the sampling costs due to the field size.

6. Conclusions

Our results show that the uncertainty in predicting the concentrations of available phosphorus and potassium in the soil was determined mainly by the number of samples used for calibration. No combination of total and calibration sample sizes that we considered would make soil spectroscopy cost-effective for determining the amounts of fertilizer to apply. Estimates from spectroscopy led to small expected losses, but the costs of data acquisition dominated the expected financial profit and loss under the ranges of sample sizes considered. However, the expected loss from for estimates of available P and K from spectroscopy for variable-rate applications of fertilizer showed a diminishing return on investment when the costs of data collection were ignored. This suggests that an optimum sample size exists provided that the cost of data acquisition could be diminished sufficiently. These findings refer to the particular situations of our study. Nevertheless, they show how the approach with the loss function can be used successfully to investigate the value of soil spectroscopy for precision agriculture.

CRediT authorship contribution statement

T.S. Breure: Writing – review & editing, Writing – original draft, Visualization, Validation, Software, Project administration, Methodology, Investigation, Formal analysis, Data curation, Conceptualization. **R. Webster:** Writing – review & editing, Writing – original draft, Validation, Supervision, Software, Resources, Methodology, Investigation, Conceptualization. **S.M. Haefele:** Writing – review & editing, Writing – original draft, Validation, Supervision, Resources, Project administration, Methodology, Investigation, Funding acquisition, Conceptualization. **J.A. Hannam:** Writing – review & editing, Writing – original draft, Validation, Supervision, Resources, Project administration, Methodology, Investigation, Funding acquisition, Conceptualization. **R. Corstanje:** Writing – review & editing, Writing – original draft, Validation, Supervision, Resources, Project administration, Methodology, Investigation, Funding acquisition, Formal analysis, Conceptualization. **A.E. Milne:** Writing – review & editing, Writing – original draft, Validation, Supervision, Software, Resources, Project administration, Methodology, Investigation, Funding acquisition, Formal analysis, Conceptualization.

Funding

Funding was provided by Biotechnology and Biological Sciences Research Council (Grant Nos. BBS/E/C/000I0320, BBS/E/C/000I0330, BBS/E/C/000I0100).

Declaration of competing interest

The authors declare that they have no known competing financial interests or personal relationships that could have appeared to influence the work reported in this paper.

Appendix A. Supplementary data

Supplementary material related to this article can be found online at https://doi.org/10.1016/j.geoderma.2025.117504.

Data availability

The authors do not have permission to share data.

References

Adamchuk, V.I., Viscarra Rossel, R.A., Marx, D.B., Samal, A.K., 2008. Enhancement of on-the-go soil sensor data using guided sampling. In: Kholsa, R. (Ed.), Proceedings of the Ninth International Conference on Precision Agriculture, Denver, Colorado, July 20–23 2008. Colorado State University, Fort Collins, Colorado, (CD publication, 13 pages).

Adamchuk, V.I., Viscarra Rossel, R.A., Marx, D.B., Samal, A.K., 2011. Using targeted sampling to process multivariate soil sensing data. Geoderma 163, 63–73.

Behrens, T., Schmidt, K., Stumpf, F., Tutsch, S., Hertzog, M., Grob, U., Keller, A., Viscarra Rossel, R., 2024. Operationalizing fine-scale soil property mapping with spectroscopy and spatial machine learning. http://dx.doi.org/10.5194/egusphere-2024-2810, EGUsphere [preprint].

Bellon-Maurel, V., McBratney, A., 2011. Near-infrared (NIR) and mid-infrared (MIR) spectroscopic techniques for assessing the amount of carbon stock in soils – Critical review and research perspectives. Soil Biol. Biochem. 43, 1398–1410.

Bivand, R., Keitt, T., Rowlingson, B., 2020. Rgdal: Bindings for the 'geospatial' data abstraction library. R package version 1.5-12. https://CRAN.R-project.org/package=rgdal. (Accessed 8 December 2020).

Bjørn-Helge, M., Wehrens, R., Hovde Liland, K., 2019. Pls: Partial least squares and principal component regression. R package version 2.7-1. https://CRAN.R-project.org/package=pls. (Accessed 5 February 2020).

Blake, L., Mercik, S., Koerschens, M., Goulding, K.W.T., Stempen, S., Weigel, A., Poulton, P.R., Powlson, D.S., 1999. Potassium content in soil, uptake in plants and the potassium balance in three European long-term field experiments. Plant Soil 216, 1–14.

Breure, T.S., Haefele, S.M., Hannam, J.A., Corstanje, R., Webster, R., Moreno-Rojas, S., Milne, A.E., 2022. A loss function to evaluate agricultural decision making under uncertainty: a case study of soil spectroscopy. Precis. Agric. 23, 1333–1353. http://dx.doi.org/10.1007/s11119-022-09887-2.

Breure, T.S., Milne, A.E., Webster, R., Haefele, S.M., Hannam, J.A., Moreno-Rojas, S., Corstanje, R., 2021. Predicting the growth of lettuce from soil infrared reflectance spectra: the potential for crop management. Precis. Agric. 22, 226–248.

Brodský, L., Vašát, R., Klement, A., Zádorová, T., Jakšík, O., 2013. Uncertainty propagation in VNIR reflectance spectroscopy soil organic carbon mapping. Geoderma 199, 54–63.

Brus, D.J., Yang, L., Zhu, A.X., 2019. Accounting for differences in costs among sampling locations in optimal stratification. Eur. J. Soil Sci. 70, 200–212.

de Gruijter, J.J., McBratney, A.B., Minasny, B., Wheeler, I., Malone, B.P., Stockmann, U., 2018. Farm-scale soil carbon auditing. In: Pedometrics. Springer, Cham, pp. 693–720.

de Gruijter, J.J., McBratney, A.B., Taylor, J., 2010. Sampling for high resolution soil mapping. In: Rossel, R.A. Viscarra, McBratney, A.B., Minasny, B. (Eds.), Proximal Soil Sensing. Springer-Verlag, New York, pp. 3–14.

Evans, J.S., 2019. Spatialeco. R package version 1.2-0, URL: https://github.com/jeffreyevans/spatialEco. (Accessed 3 October 2019).

Grafström, A., Lisic, J., 2019. Balanced sampling: Balanced and spatially balanced sampling. R package version 1.5.5, https://CRAN.R-project.org/package=BalancedSampling. (Accessed 3 November 2019).

Greenwood, D.J., Cleaver, T.J., Turner, M.K., Hunt, J., Niendorf, K.B., Loquens, S.M.H., 1980. Comparison of the effects of potassium fertilizer on the yield, potassium content and quality of 22 different vegetable and agricultural crops. J. Agric. Sci. 95, 441–456.

Guerrero, C., Zornoza, R., Gómez, I., Mataix-Beneyto, J., 2010. Spiking of NIR regional models using samples from target sites: Effect of model size on prediction accuracy. Geoderma 158, 66–77.

Hijmans, R.J., 2020. Raster: Geographic data analysis and modeling. R package version 3.3-13. https://CRAN.R-project.org/package=raster. (Accessed 8 December 2020).

Hodge, C.A.H., Burton, R.G.O., Corbett, W.M., Evans, R., Seale, R.S., 1984. Soils and their Use in Eastern England. Soil Survey of England and Wales Bulletin No. 13. Lawes Agricultural Trust, Harpenden, (Soil Survey of England and Wales).

Kennard, R.W., Stone, L.A., 1969. Computer aided design of experiments. Technometrics 11, 137–148.

Kuang, B., Mahmood, H.S., Quraishi, M.Z., Hoogmoed, W.B., Mouazen, A.M., van Henten, E.J., 2012. Sensing soil properties in the laboratory, in situ and on-line. A review. Adv. Agron. 114, 155–223.

Lark, R.M., 2000. Estimating variograms of soil properties by the method-of-moments and maximum likelihood. Eur. J. Soil Sci. 51, 717–728.

Lark, R.M., 2009. Kriging a soil variable with a simple non-stationary variance model. J. Agric. Biol. Environ. Stat. 14, 301–321.

Lark, R.M., Cullis, B.R., 2004. Model-based analysis using REML for inference from systematically sampled data on soil. Eur. J. Soil Sci. 55, 799–813.

Lark, R.M., Cullis, B.R., Weltham, S.J., 2006. On spatial prediction of soil properties in the presence of a spatial trend: the empirical best linear unbiased predictor (E-BLUP) with REML. Eur. J. Soil Sci. 57, 787–799.

Lark, R.M., Knights, K.V., 2015. The implicit loss function for errors in soil information. Geoderma 251–252, 24–32.

Lark, R.M., Marchant, B.P., 2018. How should a spatial coverage sampling design for a geostatistical soil survey be supplemented to support estimation of spatial covariance parameters? Geoderma 319, 89–99.

Milne, R., Mobbs, D.C., Thomson, A.M., Matthews, R.W., Broadmeadow, M.S.J., Mackie, E., Wilkinson, M., Benham, S., Harris, K., Grace, J., Quegan, S., Coleman, K., Powlson, D.S., Whitmore, A.P., Sozanska-Stanton, M., Smith, P., Levy, P.E., Ostle, N., Murray, T.D., Van Oijen, M., Brown, T., 2006. UK Emissions By Sources and Removals By Sinks Due To Land Use, Land Use Change and Forestry Activities. Report, April 2006. (CEH Project Report Number C02275), Centre for Ecology and Hydrology, Wallingford, United Kingdom, p. 278, http://nora.nerc.ac.uk/3370/.

Minasny, B., McBratney, A.B., Walvoort, D.J.J., 2007. The variance quadtree algorithm: Use for spatial sampling design. Comput. Geosci. 33, 383–392.

Muhammed, S.E., Marchant, B.P., Webster, R., Whitmore, A.P., Dailey, G., Milne, A.E., 2017. Assessing sampling design for determining fertilizer practice from yield data. Comput. Electron. Agric. 135, 163–174.

Papritz, A., 2025. georob: Robust Geostatistical Analysis of Spatial Data. R package version 0.3.23, https://CRAN.R-project.org/package=georob. (Accessed 25 September 2025).

Pebesma, E., 2018. Simple features for R: Standardized support for spatial vector data. R J. 10, 439–446.

Prasad, M., Spiers, T.M., Ravenwood, I.C., 1988. Target phosphorus soil test values for vegetables. N. Z. J. Exp. Agric. 16, 83–90.

Ramirez-Lopez, L., Wadoux, A.M.J.-C., Franceschini, M.H.D., Terra, F.S., Marques, K.P.P., Sayão, V.M., Demattê, J.A.M., 2019. Robust soil mapping at the farm scale with vis–NIR spectroscopy. Eur. J. Soil Sci. 70, 378–393.

Ribeiro, Jr., P.J., Diggle, P.J., 2018. geoR: Analysis of geostatistical data. R package version 1.7-5.2.1. https://CRAN.R-project.org/package=geoR. (Accessed 5 February 2020).

Savitzky, A., Golay, M.J.E., 1964. Smoothing and differentiation of data by simplified least squares procedures. Anal. Chem. 36, 1627–1639.

Schmidt, K., Behrens, T., Daumann, J., Ramirez-Lopez, L., Werban, U., Dietrich, P., Scholten, T., 2014. A comparison of calibration sampling schemes at the field-scale. Geoderma 232, 243–256.

Shaw, R., Lark, R.M., Williams, A.P., Chadwick, D.R., Jones, D.L., 2016. Characterising the within-field scale spatial variation of nitrogen in a grassland soil to inform the efficient design of in-situ nitrogen sensor networks for precision agriculture. Agricult. Ecosys. Environ. 230, 294–306. http://dx.doi.org/10.1016/j.agee.2016.06.004.

Soriano-Disla, J.M., Janik, L.J., Viscarra Rossel, R.A., Macdonald, L.M., McLaughlin, M.J., 2013. The performance of visible, near-, and mid-infrared reflectance spectroscopy for prediction of soil physical, chemical, and biological properties. Appl. Spectrosc. Rev. 49, 139–186. http://dx.doi.org/10.1080/05704928.2013.811081.

Stevens, A., Ramirez-Lopez, L., 2013. An introduction to the prospectr package. R package Vignette R package version 0.1.3, URL: https://cran.r-project.org/package=prospectr. (Accessed 3 October 2019).

Viscarra Rossel, R.A., Adamchuk, V.I., Sudduth, K.A., McKenzie, N.J., Lobsey, C., 2011. Proximal soil sensing. An effective approach for soil measurements in time and space. Adv. Agron. 113, 237–282.

Viscarra Rossel, R.A., Behrens, T., Ben-Dor, E., Chabrillant, S., Demattê, J.A.M., Ge, Y., Gomez, C., Guerrero, C., Peng, Y., Ramirez-Lopez, R., Shi, Z., Webster, R., Winowiecki, L., Shen, Z., 2022. Diffuse reflectance spectroscopy for estimating soil properties: a technology for the 21st century. Eur. J. Soil Sci. 73, e13271. http://dx.doi.org/10.1111/ejss.13271.

Viscarra Rossel, R.A., Brus, D.J., Lobsey, C., Shi, Z., McLachlan, G., 2016. Baseline estimates of soil organic carbon by proximal sensing: comparing design-based, model-assisted and model-based inference. Geoderma 265, 152–163.

Viscarra Rossel, R.A., Walvoort, D.J.J., McBratney, A.B., Janik, L.J., Skjemstad, J.O., 2006. Visible, near infrared, mid infrared or combined diffuse reflectance spectroscopy for simultaneous assessment of various soil properties. Geoderma 131, 59–75.

Wadoux, A.M.J.-C., Marchant, B.P., Lark, R.M., 2019. Efficient sampling for geostatistical surveys. Eur. J. Soil Sci. 70, 975–989.

Walvoort, D.J.J., Brus, D.J., de Gruijter, J.J., 2010. An R package for spatial coverage sampling and random sampling from compact geographical strata by *k*-means. Comput. Geosci. 36, 1261–1267.

Webster, R., Oliver, M.A., 1992. Sample adequately to estimate variograms of soil properties. J. Soil Sci. 43, 177–192.

Webster, R., Oliver, M.A., 2007. Geostatistics for Environmental Scientists, second ed. John Wiley & Sons, Chichester.

Weiss, C.E., Roetzer, G.R., 2016. GeomComb: (Geometric) forecast combination methods. R package version 1.0. URL: https://CRAN.R-project.org/package=GeomComb. (Accessed 05 March 2020).

Wickham, H., 2016. Ggplot2: Elegant Graphics for Data Analysis. Springer-Verlag, New York, https://ggplot2.tidyverse.org. (Accessed 14 February 2020).

Wickham, H., Averick, M., Bryan, J., Chang, W., McGowan, L.D'A., François, R., et al., 2019. Welcome to the tidyverse. J. Open Source Softw. 4 (1686).

Yates, F., 1981. Sampling Methods for Censuses and Surveys, fourth ed. Griffin, London.